Experimental and numerical investigation of the hetero-/homogeneous combustion of lean propane/air mixtures over platinum

Symeon Karagiannidis [a], John Mantzaras [a,*], Rolf Bombach [a],
Sabine Schenker [a], Konstantinos Boulouchos [b]

[a] *Paul Scherrer Institute, Combustion Research, CH-5232 Villigen-PSI, Switzerland*
[b] *Swiss Federal Institute of Technology, Laboratory of Aerothermochemistry and Combustion Systems,
CH-8092 Zurich, Switzerland*

Abstract

The pure heterogeneous and the coupled hetero-/homogeneous combustion of fuel-lean propane/air mixtures over platinum have been investigated at pressures $1 \, bar \leqslant p \leqslant 7 \, bar$, fuel-to-air equivalence ratios $0.23 \leqslant \varphi \leqslant 0.43$, and catalytic wall temperatures $723 \, K \leqslant T_w \leqslant 1286 \, K$. Experiments were performed in an optically accessible catalytic channel-flow reactor and involved 1-D Raman measurements of major gas-phase species concentrations across the reactor boundary layer for the assessment of catalytic fuel conversion and planar laser induced fluorescence (LIF) of the OH radical for the determination of homogeneous ignition. Numerical predictions were carried out with a 2-D elliptic CFD code that included a one-step catalytic reaction for the total oxidation of propane on Pt, an elementary C_3 gas-phase chemical reaction mechanism, and detailed transport. A global catalytic reaction step valid over the entire pressure–temperature-equivalence ratio parameter range has been established, which revealed a $\sim p^{0.75}$ dependence of the catalytic reactivity on pressure. The aforementioned global catalytic step was further coupled to a detailed gas-phase reaction mechanism in order to simulate homogeneous ignition characteristics in the channel-flow reactor. The predictions reproduced within 10% the measured homogeneous ignition distances at pressures $p \leqslant 5 \, bar$, while at $p = 7 \, bar$ the simulations overpredicted the measurements by 19%. The overall model performance suggests that the employed hetero-/homogeneous chemical reaction schemes are suitable for the design of propane-fueled catalytic microreactors.
© 2009 The Combustion Institute. Published by Elsevier Inc. All rights reserved.

Keywords: Catalytic combustion of propane on platinum; Hetero-/homogeneous combustion; Pressure dependence of catalytic reactivity; Homogeneous ignition

1. Introduction

Catalytic combustion is being pursued in large power generation systems as an ultra-low-NO_x technology with enhanced flame stability under either fuel-lean or fuel-rich operating conditions [1–3]. Methane, the main constituent of natural

* Corresponding author. Fax: +41 56 3102199.
 E-mail address: ioannis.mantzaras@psi.ch (J. Mantzaras).

gas, has been the fuel of interest in the aforementioned studies. The catalytic combustion of higher hydrocarbons and of hydrogen has attracted increased attention during the last years for the portable production of energy and heat using micro- and mesoscale power devices [4–6].

Propane is a fuel of particular interest for micro-energy conversion systems since it liquefies at room temperature and moderate pressures and is commercially available in compact containers for numerous consumer applications. The study of its complete oxidation over catalytic surfaces constitutes a natural first step towards understanding the similar behavior of higher hydrocarbons. Some of the physical characteristics of propane are common among higher hydrocarbons, such as the larger-than-unity Lewis number (a property directly impacting the catalyst surface temperatures [7,8]) and the negative temperature coefficient of the gas-phase ignition characteristics under certain operating conditions.

On a fundamental level, the oxidation of propane over noble metals at atmospheric pressure has been studied along with higher and lower hydrocarbons [9,10], with the latter study employing a non-activated dissociative chemisorption step for propane and a temperature-dependent adsorption/desorption reaction set for oxygen. It has been shown that the catalytic reactivity of linear alkanes increases with increasing carbon chain length, due to weaker C—C bond strengths of higher hydrocarbons; in addition, platinum is the most active noble metal for the oxidation of all alkanes except methane [11]. Detailed heterogeneous reaction mechanisms for fuel-lean combustion of higher hydrocarbons have not yet progressed to the same extent as those of methane [12,13]. Recent studies of fuel-lean propane oxidation over Pt-based catalysts suggested an overall reaction that is first order with respect to propane and zero-th order with respect to oxygen [14]. Accompanying experiments of propane catalytic combustion have mainly been conducted at atmospheric pressure [4,6,15].

We have recently [16] investigated numerically the stability maps of methane-fueled catalytic microreactors at pressures up to 5 bar, a range of interest to microturbine-based power generation systems. Detailed hetero-/homogeneous reaction schemes were used, validated over the appropriate pressure and temperature ranges with in situ laser-based spectroscopic measurements [17–19]. The former study [16] exemplified the importance of gas-phase chemistry and of high operating pressure for extending the combustion stability limits of microreactors, while the latter [17,18] have also addressed the implications of using global catalytic reaction steps in modeling methane hetero-/homogeneous combustion under high pressures.

The present work undertakes a combined experimental and numerical investigation of the catalytic combustion of fuel-lean C_3H_8/air mixtures over platinum at pressures $1 \leqslant p \leqslant 7$ bar, a range of interest to microreactors and small-scale industrial turbines. Experiments have been carried out in an optically accessible, channel-flow catalytic reactor at propane-to-air equivalence ratios ranging between 0.23 and 0.43. The heterogeneous reactivity is assessed with Raman spectroscopy of major gas-phase species concentrations across the channel boundary layer, and the onset of homogeneous ignition is monitored with planar laser induced fluorescence (LIF) of the OH radical. Simulations are performed with a full elliptic 2-D CFD code. The main objectives are to assess the catalytic reactivity of propane and its pressure dependence by constructing an appropriate global reaction step and then to couple this step with a detailed homogeneous reaction mechanism so as to reproduce the measured homogeneous ignition characteristics.

2. Experimental

2.1. High pressure test rig

The test-rig (Fig. 1) consisted of a channel-flow catalytic reactor, which was mounted inside a high-pressure cylindrical tank. The reactor comprised two horizontal Si[SiC] plates with a length (x) of 300 mm, width (z) of 110 mm and thickness of 9 mm; the plates were positioned 7 mm apart (y). The other two sides of the reactor were formed by two 3-mm-thick vertical quartz windows. The inner surfaces of the Si[SiC] plates were coated via plasma vapor deposition with a 1.5 μm thick Al_2O_3 non-porous layer, followed by a 2.2 μm thick platinum layer. BET and CO-chemisorption measurements verified the absence of porous structure in the catalyst layer [17]. The sur-
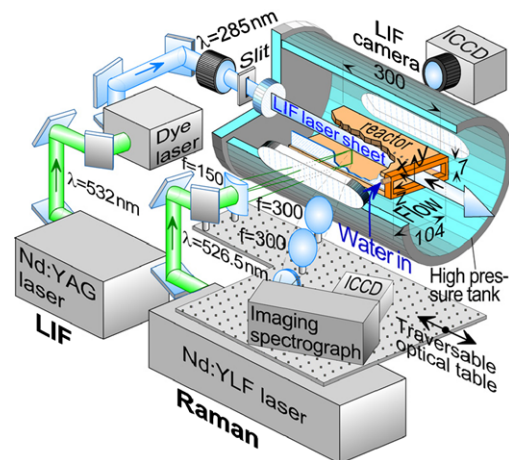

Fig. 1. Test rig and Raman/LIF setup.

face temperatures along the x–y symmetry plane were monitored with S-type thermocouples (12 for each plate), which were embedded 0.9 mm beneath the catalyst layer. To facilitate the catalytic reactivity studies, a kinetically controlled fuel conversion away from the mass-transport-limit was necessary. To avoid transport limitations originating from the high catalytic reactivity of propane over platinum, a coupled cooling/heating arrangement was adopted to control the surface temperatures: in a fashion similar to earlier hydrogen catalytic combustion studies [20], the reactor entry section was water-cooled to maintain a low catalytic reactivity while the rear of the reactor ($x > 100$ mm) was heated by two resistive heaters placed above the ceramic plates.

A compressor provided dry air, which was preheated and mixed with propane (Grade 3.5 purity) in two sequential static mixers. The preheated propane/air mixture was driven into the reactor through a 50-mm long inert rectangular honeycomb section that provided a uniform inlet velocity profile. The reactor inlet temperature was monitored with a thermocouple placed downstream of the honeycomb section. The high-pressure vessel was fitted with two 350-mm long and 35-mm thick quartz windows (see Fig. 1), which maintained optical accessibility from both reactor sides. Two additional quartz windows located at the exhaust section of the vessel and the reactor outlet provided a counterflow optical access for the LIF experiments. Apart from propane/air, experiments with propane/air/oxygen mixtures have also been carried out.

2.2. Laser diagnostics

The LIF/Raman set-up is also shown in Fig. 1. The particularly low volumetric content of fuel in lean propane/air combustion necessitated the use of a dedicated high power laser for the Raman measurements. The 526.5 nm radiation of a frequency-doubled Nd:YLF high repetition rate pulsed laser (Quantronix Darwin Duo), operated at 1.5 to 2 kHz, with a pulse duration and energy of 130 ns and 37 to 43 mJ, respectively, provided the light source for the Raman measurements. Given the laminar and steady operating conditions, the signal of 20,000 to 40,000 pulses was integrated on the detector chip when acquiring an image. Six of these images were subsequently averaged, such that up to 9 kJ of laser light was used for a single Raman spectrum. The signal-to-noise ratio was thus increased by a factor of 20 compared to the previous methane/air Raman arrangement [18,19]; moreover, the danger of dielectric gas breakdown was eliminated due to the resulting lower intensities at the focal line.

The 526.5 nm beam was focused through the tank and reactor side-windows into a vertical line

($\sim$0.3 mm thick) by an $f = 150$ mm cylindrical lens. The focal line spanned the 7 mm channel separation and was offset laterally ($z = 15$ mm) to increase the collection angle and minimize thermal beam steering [19]. Two $f = 300$ mm lenses collected the scattered light at a 50° angle with respect to the incident optical path and focused it to the entrance slit of a 25 cm imaging spectrograph (Chromex-250i) equipped with an intensified CCD camera (Princeton Instruments PI-MAX1024GIII). The 1024- and 256-pixel-long CCD dimensions corresponded to wavelength and transverse distance, respectively. The effective Raman cross sections, which included transmission efficiencies, were evaluated by recording the signals of pure propane, air, and completely burnt gases of known composition. Raman data for the major combustion species C_3H_8, H_2O, N_2, O_2, and CO_2 were acquired at different positions by traversing axially a table supporting the sending and collecting optics and also the Nd:YLF laser (Fig. 1). The 250-pixel-long 7 mm channel height was binned to 63 pixels.

For the OH-LIF, the 532 nm radiation of a frequency-doubled Nd:YAG laser (Quantel TDL90 NBP2UVT3) pumped a tunable dye laser (Quantel TDL90); its frequency-doubled radiation (285 nm) had a pulse energy of 0.5 mJ, low enough to avoid saturation of the $A(v = 1) \leftarrow X(v' = 0)$ transition. The 285 nm beam was transformed into a laser sheet by a cylindrical lens telescope and a 1 mm slit mask, which propagated counterflow, along the x–y symmetry plane (Fig. 1). The fluorescence of both (1–1) and (0–0) transitions at 308 and 314 nm, respectively, was collected at 90° (through the reactor and tank side-windows) with an intensified CCD camera (LaVision Imager Compact HiRes IRO, 1392 × 1024 pixels binned to 696 × 512). A $120 × 7$ mm^2 section of the combustor was imaged on a $600 × 34$ pixel CCD-area. The camera was traversed axially to map the 300 mm reactor extent; at each measuring location 400 images were averaged.

3. Numerical

The lack of detailed surface reaction mechanisms for propane on platinum necessitated the use of a single-step catalytic reaction coupled to a detailed gas-phase reaction mechanism. The global reaction step of Garetto et al. [14] has been developed for the total oxidation of propane to H_2O and CO_2 over Pt at atmospheric pressure, for a range of equivalence ratios encompassing the conditions of this work:

$$\dot{s}_{C_3H_8} = A \times T_w^{1.15} \times \exp(-E_a/RT_w) \times [C_3H_8]_w^\alpha.$$

(1)

The catalytic rate $\dot{s}_{C_3H_8}$ is in [mol/cm^{2}s], $A = 93.2$ K$^{-1.15}$ cm$^{1.45}$ mol$^{-0.15}$ s^{-1}, $E_a = 71.128$ kJ/mol, $a = 1.15$ and the concentration of propane [C_3H_8] is in [mol/cm^3]. Finally, the subscript w denotes conditions at the gas–wall interface.

An optimized mechanism for homogeneous combustion of C_1–C_3 species by Qin et al (70 species, 14 irreversible and 449 reversible reactions) [21] was employed for modeling gas-phase chemistry. Thermodynamic data were included in the provided scheme. Surface and gas-phase reaction rates were evaluated with Surface-CHEMKIN [22] and CHEMKIN [23], respectively. Mixture-average diffusion was the transport model, using the CHEMKIN transport database [24].

A steady, full-elliptic, 2-D laminar CFD code was used in the simulations (for details see [19]). An orthogonal staggered grid of 450 × 140 points (x and y, respectively) was sufficient to give a grid independent solution for the 300 × 7 mm^2 channel domain. Uniform inlet profiles were applied for temperature, axial velocity and species mass fractions. The interfacial energy boundary conditions were prescribed wall temperature profiles; these profiles were polynomial curves fitted through the thermocouple measurements of the upper and lower walls. No-slip was applied for both velocity components at the walls ($y = 0$ and 7 mm), while zero-Neumann conditions were used at the outlet.

4. Results and discussion

The experimental conditions are provided in Table 1. The inlet Reynolds numbers, Re_{IN}, (based on the uniform inlet properties and the channel hydraulic diameter) were as high as 2171, leading to laminar flows; recent turbulent catalytic combustion studies [25] have shown that the strong flow laminarization induced by the hot

Table 1
Experimental conditions[a]

Case	P	φ	T_{IN}	U_{IN}	Re_{IN}	N_2 vol.%
1	1	0.30	398	1.45	827	55
2	3	0.27	400	1.10	1831	60
3	5	0.27	399	0.66	1836	60
4	7	0.26	398	0.55	2162	60
5	3	0.31	446	1.58	2171	77
6	5	0.23	448	0.94	2162	55
7	7	0.31	446	0.68	2170	77
8	1	0.43	492	1.39	544	77
9	3	0.42	468	0.51	655	77
10	5	0.43	478	0.28	571	77
11	7	0.42	475	0.29	859	77

[a] Pressure, equivalence ratio, inlet temperature, velocity, Reynolds number and nitrogen dilution. Cases with 77% vol. N_2 pertain to C_3H_8/air mixtures.
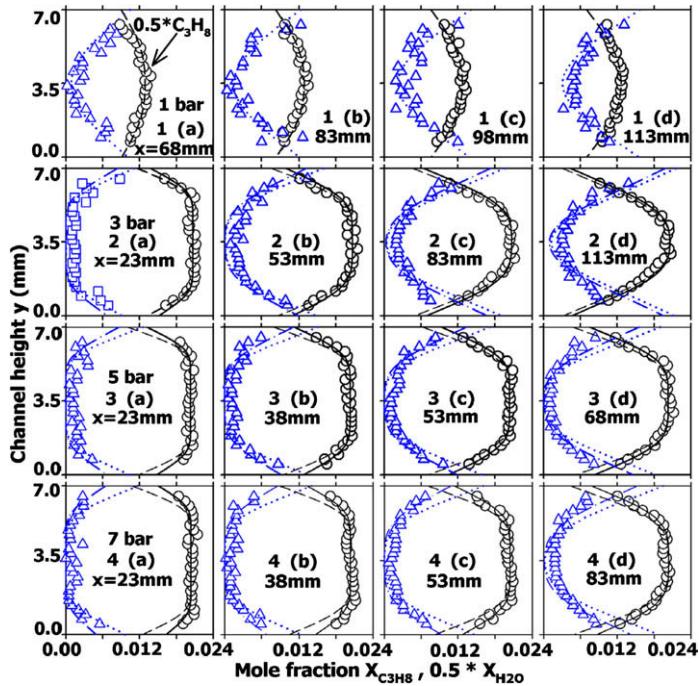
catalytic walls guarantees laminar flow conditions at considerably higher Re_{IN}. Cases 1–7, characterized by the absence of homogeneous ignition, provided the platform for evaluating the catalytic reactivity and its pressure dependence with the aid of the Raman measurements. In Cases 8–11, whereby flames were established inside the channel, the gas-phase combustion processes were evaluated using the OH-LIF data.

4.1. Effect of pressure on the catalytic reactivity

Comparisons between Raman-measured and predicted transverse profiles of C_3H_8 and H_2O mole fractions, at four selected streamwise locations, are illustrated in Fig. 2 for Cases 1–4; for clarity, 27 of the total 63 measured points are provided. Modest profile asymmetries are evident due to small differences between the upper- and lower-wall temperatures (see the wall temperatures of Fig. 3). The experimentally resolved transverse extent ranged from $0.3 \leqslant y \leqslant 6.7$ mm at high pressures down to $0.6 \leqslant y \leqslant 6.4$ mm for the atmospheric pressure experiments (due to the increasing Raman signal-to-noise ratio with rising pressure). The measurement accuracy was ±10% for compositions as low as 0.5% vol.; concentrations less than 0.5% vol. entailed larger measurement uncertainties. To further increase the Raman signal of the deficient reactant (propane), C_3H_8/air/O_2 mixtures were also examined in certain cases, whereby the volumetric content of nitrogen was as low as 55%. Axial profiles of the computed catalytic (C) and gas-phase (G) propane conversion rates (the latter integrated over the 7-mm channel height), are presented in Fig. 3 for Cases 1–4. The maximum reactor extent over which the G conversion is negligible has been delineated with the arrows in Fig. 3 (defined as the positions where the G conversion amounts to 5% of the C conversion). For the assessment of the catalytic reactivity, the forthcoming comparisons of Raman data with predictions are limited to this extent so as to avoid falsification of the catalytic kinetics by gas-phase chemistry. The initial reactor extent over which the gas-phase contribution could be safely neglected ranged from 10.9 cm (Case 3) to 14.2 cm (Case 4).

The heterogeneous reactivity of propane was assessed by varying the reactor pressure and surface temperature, and monitoring the near-wall bending of the propane transverse profiles. In Case 2 (Fig. 2, $p = 3$ bar) the catalytic fuel conversion is already appreciable at surface temperatures $T_w \leqslant 850$ K, while mass-transport-limited conditions are approached for $T_w = 1064$ K (manifested by the low propane mole fractions near both walls in Fig. 2(d)). In contrast, previous CH_4/air studies [18] in the same reactor necessitated an increase in pressure to achieve a similar level of reactivity under the same mass inflowcon-

Fig. 2. Measured and predicted transverse profiles of C_3H_8 and H_2O mole fractions for Cases 1–4 at four streamwise locations. Measurements: C_3H_8 (circles), H_2O (triangles). Predictions: C_3H_8 (solid lines, pressure-corrected model; dashed lines, Garetto), H_2O (dashed-dotted lines, pressure-corrected model; dotted lines, Garetto).

ditions. Numerical predictions using the global catalytic reaction rate of Garetto yielded a very good agreement with the measured C_3H_8 and H_2O profiles at pressures up to 3 bar (Fig. 2). Moreover, the increase in catalytic reactivity with increasing downstream surface temperatures and the approach to transport-limited conversion is also well captured at this pressure range (see Fig. 2(2a) through (2d)).

At pressures above 3 bar, the employed catalytic model could not capture the measured boundary-layer profile of propane (see Fig. 2(3 and 4)); therein, the predictions clearly overpredicted the measured catalytic reactivity. This is attributed to the overall reaction order (and hence pressure order) of 1.15 (Eq. (1)). Recent catalytic combustion studies of methane on Pt [18] have shown that the heterogeneous reactivity of methane follows a $\sim p^{0.47}$ pressure dependence, over the range $1 \leqslant p \leqslant 16$ bar; this power law bears the combined effects of the first-order reaction dependence with respect to methane, and the $p^{-0.53}$ dependence due to the reduction of free platinum sites with increasing oxygen partial pressure. The latter mechanism is very important in restraining the rate of increase of the catalytic reactivity with rising pressure. The challenge in a global catalytic step is to reproduce the reactivity over a wide range of operating conditions (pres-

sures and temperatures). Appropriate pressure corrections have thus been proposed for global catalytic steps of methane [18]; with such corrections, the performance of single steps has been shown to be modest over the wide pressure range 1 to 16 bar.

In a fashion similar to the earlier methane studies, the current global propane step is extended by introducing a pressure term which restrains the rate of increase of the catalytic reactivity with increasing pressure:

$$\dot{s}_{C_3H_8} = A \times \left(\frac{p}{p_0}\right)^{-n} T_w^{1.15} \times \exp(-E_a/RT_w) \times [C_3H_8]^\alpha,$$

(2)

with n a positive number smaller than unity, and $p_0 = 1$ bar. A value of $n = 0.4 \pm 0.03$ yielded the best fit to the experimentally acquired boundary layer propane profiles over the entire pressure range $1 \leqslant p \leqslant 7$ bar, for all the cases considered in this work (Fig. 2).

Transverse profiles of major species were computed anew for Cases 2–4 with the proposed kinetics of Eq. (2) at locations upstream of considerable gas-phase fuel conversion. Significantly better agreement with the Raman data was achieved for the higher pressure Cases 3 and 4 (5 and 7 bar, respectively) as seen in Fig. 2, particularly for the
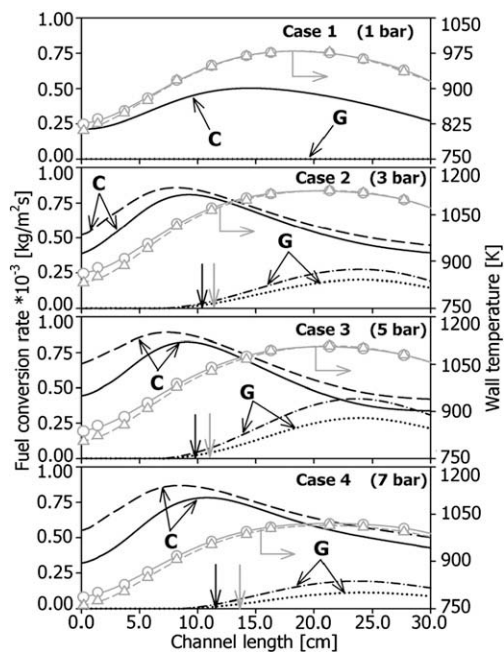
Fig. 3. Computed streamwise catalytic (C) and gas-phase (G) fuel conversion rates, averaged over y (solid, dashed-dotted-lines: pressure-corrected model; dashed, dotted-lines: Garetto). Upper- and lower-wall (solid and dashed gray lines respectively) temperature profiles fitted through thermocouple measurements (upper: circles; lower: triangles). The vertical arrows on the x-axes define the onset of non-negligible gas-phase conversion (black: pressure-corrected model; gray: Garetto).

lower examined surface temperatures. At the same time, the good model performance at pressures $p \leqslant 3$ bar was retained. The large overprediction of catalytic reactivity by Eq. (1) is evident in Fig. 3. For Case 4 (7 bar), the fuel conversion rate is overpredicted by as much as 42% for a surface temperature of 786 K, which in turn yields the same overprediction in heterogeneously-produced water (Fig. 2(4)). At higher wall temperatures, however, mass-transport-limited operation is approached and both models yield similar results: the difference between both model predictions drops to 5.2% at 995 K. It is noted that the enhanced performance of Eq. (2) yielded a more conservative estimate of the reactor extent with minimal gas-phase contribution. As seen in Fig. 3, the computed lengths of significant gas-phase conversion are reduced by as much as 13 and 21 mm for Cases 3 and 4, respectively. The associated higher near-wall fuel concentration, along with the increased concentration of catalytically produced water in the gas-phase induction zone, have been shown to affect the onset of homogeneous ignition [19].

The applicability of the pressure-corrected global step was further evaluated by comparing numerically predicted species profiles with Raman data for Cases 5–7 (Fig. 4). The propane and water profiles are captured correctly at all pressures and for all surface temperatures considered. Cases 5 and 7 pertain to propane/air mixtures (without oxygen addition) with same equivalence ratio and mass inflow and similar surface temperatures, at 3 and 7 bar, respectively. An increased catalytic reactivity from 3 to 7 bar is evident by comparing propane profiles at position $x = 68$ mm, with upper wall temperatures of 864 and 868 K for Cases 5 and 7, respectively. Case 6 is provided to exemplify the aptness of the extended model at lower equivalence ratios ($\phi = 0.23$) and lower wall temperatures (723 K $\leqslant T_{wall} \leqslant$ 898 K).

4.2. Homogeneous ignition

It can be argued that a global catalytic step that captures (over a prescribed range of operating parameters) the heterogeneous fuel consumption, when used in conjunction with a detailed
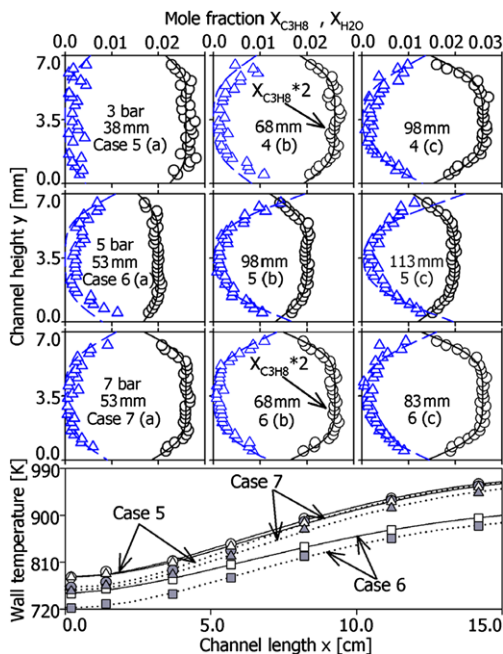

Fig. 4. Measured and predicted transverse profiles of C_3H_8 and H_2O mole fractions for Cases 5, 6, and 7 at three streamwise locations. Measurements: C_3H_8 (circles), H_2O (triangles). Predictions: C_3H_8, solid lines; H_2O, dashed-dotted lines. For clarity, the scale of propane has been expanded by a factor of 2 in Cases 5 and 7. Upper- and lower-wall (solid and dotted-lines, respectively) temperature profiles fitted through thermocouple measurements (upper: open symbols; lower: gray-filled symbols) for Cases 5 (circles), 6 (squares), and 7 (triangles).

homogeneous reaction scheme, can also reproduce the onset of homogeneous ignition. Earlier catalytic combustion studies of hydrogen and methane [19,20] with detailed hetero-/homogeneous reaction schemes have clarified the particularly weak coupling between the two pathways via radical adsorption/desorption reactions; this coupling had a minimal effect on the radical pool over the gas-phase induction zone [19,20,26]. Major hetero-/homogeneous interactions come from the near-wall catalytic fuel depletion, which in turn inhibits homogeneous ignition [7], and a secondary chemical coupling originating from the heterogeneously produced major species (notably H_2O), which impact homogeneous ignition (promoting for methane [17,27], inhibiting for hydrogen [20,28]). These two effects can be captured by a global catalytic step. Coupling via other intermediate species, such as CO, can be important [16,18] in determining the overall consumption of this species and in determining the resulting CO emissions but its impact on homogeneous ignition of methane is secondary [17]. Previous hydrogen and methane homogeneous ignition studies have clearly pointed out that deficiencies in homogeneous ignition predictions stem mostly from low-temperature gas-phase kinetics and not from heterogeneous kinetics [17,20].

Comparisons between LIF-measured and numerically predicted distributions of the OH radical are illustrated in Fig. 5 for Cases 8–11 of Table 1. In all cases, the pressure-corrected heterogeneous model established in the previous section was used, coupled to the optimized gas-phase mechanism of Qin. The slight asymmetries of the flames are due to temperature differences between the two catalytic walls. The location of homogeneous ignition (x_{ig}), shown with the green arrows in Fig. 5, was determined in both experiments and predictions as the streamwise position where OH levels rose to 5% of their maximum flame values. The OH color-coded bars (ppmv) in Fig. 5 refer to the predictions (the OH-LIF measurements were in the linear regime but absolute concentrations were not deduced). The lower pressure flames exhibited the highest absolute OH levels, which dropped rapidly with increasing pressure.

Having established the applicability of the pressure-corrected global step in the previous section, the comparisons in Fig. 5 allow for a direct evaluation of the gas-phase reaction scheme in predicting ignition delay times and laminar flame speeds (linked to the homogeneous ignition distances and to the flame sweep angles inside the channel, respectively). Figure 5 indicates a moderate ability of the gaseous scheme in capturing correctly the measured flame shapes, with better agreement at lower pressures. However, of greater importance is the ability of the gaseous scheme to correctly predict homogeneous ignition distances (since homogeneous ignition is deemed as detrimental to the reactor integrity). An overall good agreement is achieved between measurements and predictions; the ignition distance is underpredicted by 9.3% for Case 8 (1 bar), while pressures up to 5 bar consistently yielded overpredictions (by up to 9.8% for Case 10). Increasing the pressure to 7 bar resulted in greater overpredictions of x_{ig} (by 19% for Case 11). These observations are in accordance with recent numerical studies that demonstrated the gas-phase mechanism's inability to correctly capture measured ignition delay times of propane at moderate-to-high pressures ($p > 4$ bar) [29].

Further validation for the applicability of the coupled hetero-/homogeneous models is provided in Fig. 6; Raman-measured major species profiles over the channel half-height are compared against
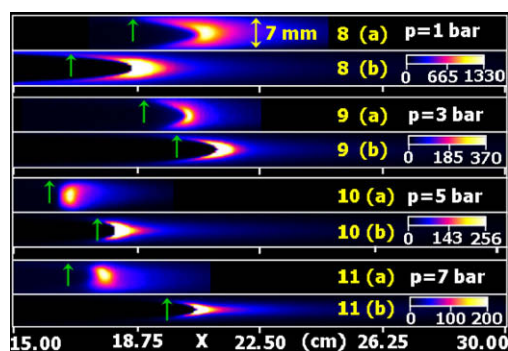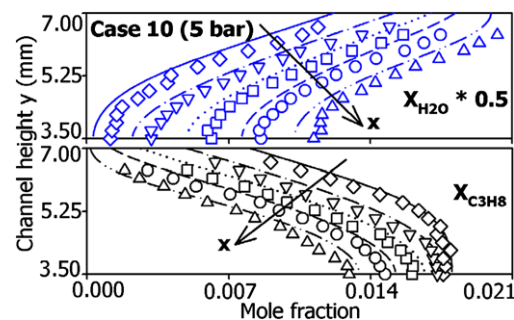
Fig. 5. Measured and predicted distributions of the OH radical for Cases 8–11. (a) OH-LIF, (b) numerical predictions with the Qin (gas-phase) and pressure-corrected (catalytic) reaction schemes. The green arrows define the onset of homogeneous ignition. Predicted OH levels in ppmv.

Fig. 6. Predicted (lines) and measured (symbols) profiles over the channel half-height of C_3H_8 and H_2O mole fractions for Case 10 at streamwise positions $x = 23$ (solid lines, diamonds), 53 (dashed-dotted lines, lower triangles), 83 (dotted lines, squares), 113 (dashed lines, circles), and 143 (dashed-doubled-dotted lines, upper triangles) mm.
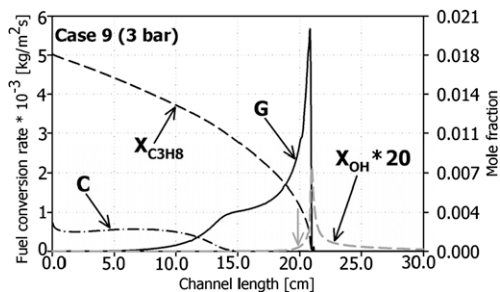
Fig. 7. Predicted catalytic (C) and gas-phase (G) conversion rates for the entire channel length for Case 9, along with propane and OH radical species mole fractions. The vertical gray arrow on the x-axis indicates the predicted point of homogeneous ignition.

numerical predictions obtained using the pressure-corrected global step and the gas-phase scheme, for selected streamwise positions of Case 10 prior to homogeneous ignition. The predictions are in good agreement with the experiments, indicating that the chemical models capture correctly the fuel consumption in the reactor.

In Fig. 7, catalytic and gas-phase conversion rates along with propane and OH radical mole fractions are plotted for Case 9. It is evident that gas-phase chemistry is responsible for most of the fuel conversion, well-before the onset of homogeneous ignition. Specifically, the pre-ignition gas-phase chemistry already surpasses the catalytic chemistry in terms of fuel conversion at $x = 11.8$ cm, whereby only $\sim32\%$ of the fuel has been converted. The significant amount of fuel available for homogeneous reactions is due to the small surface-to-volume ratio of the channel (dictated by requirements of reactor optical accessibility), along with the large Lewis number of propane that in turn reduces the fuel transport rate to the catalytic surfaces.

5. Conclusions

The pure heterogeneous and the coupled hetero-/homogeneous combustion of lean propane/air mixtures over platinum was investigated experimentally in an optically accessible, channel flow reactor at pressures 1 bar $\leqslant p \leqslant$ 7 bar with in situ, 1-D Raman and planar OH-LIF measurements. The catalytic fuel conversion rate was assessed as a function of pressure, equivalence ratio and surface temperature. A global-step catalytic reaction for propane was established, which correctly accounted for the pressure dependence of the catalytic reactivity over the entire investigated pressure range. Numerical predictions using a detailed homogeneous reaction scheme coupled with the established catalytic reaction step repro-

duced the onset of gas-phase ignition at moderate pressures ($p \leqslant 5$ bar), with somewhat more pronounced overpredictions at higher pressures (7 bar). The overall performance of the employed hetero-/homogeneous reaction models verified their applicability for the design of propane-fueled catalytic microreactors.

Acknowledgments

Appendix A. Supplementary data

Supplementary data associated with this article can be found, in the online version, at doi:10.1016/j.proci.2008.06.063.

References

[1] R. Carroni, V. Schmidt, T. Griffin, Catal. Today 75 (2002) 287–295.
[2] A. Schneider, J. Mantzaras, R. Bombach, S. Schenker, N. Tylli, P. Jansohn, Proc. Combust. Inst. 31 (2007) 1973–1981.
[3] L.L. Smith, H. Karim, M.J. Castaldi, S. Etemad, W.C. Pfefferle, Catal. Today 117 (2006) 438–446.
[4] J.M. Ahn, C. Eastwood, L. Sitzki, P.D. Ronney, Proc. Combust. Inst. 30 (2005) 2463–2472.
[5] A. Gomez, J.J. Berry, S. Roychoudhury, B. Coriton, J. Huth, Proc. Combust. Inst. 31 (2007) 3251–3259.
[6] D.G. Norton, D.G. Vlachos, Proc. Combust. Inst. 30 (2005) 2473–2480.
[7] J. Mantzaras, Interplay of transport and hetero-/homogeneous chemistry, in: S.Z. Jiang (Ed.), Focus on Combustion Research, Nova Publishers, New York, 2006, p. 241.
[8] W.C. Pfefferle, L.D. Pfefferle, Prog. Energy Combust. Sci. 12 (1986) 25–41.
[9] G. Veser, M. Ziauddin, L.D. Schmidt, Catal. Today 47 (1999) 219–228.
[10] S.R. Deshmukh, D.G. Vlachos, Combust. Flame 149 (2007) 366–383.
[11] M. Aryafar, F. Zaera, Catal. Lett. 48 (1997) 173–183.
[12] O. Deutschmann, L.I. Maier, U. Riedel, A.H. Stroemman, R.W. Dibble, Catal. Today 59 (2000) 141–150.
[13] P. Aghalayam, Y.K. Park, N. Fernandes, V. Papavassiliou, A.B. Mhadeshwar, D.G. Vlachos, J. Catal. 213 (2003) 23–38.
[14] T.F. Garetto, E. Rincon, C.R. Apesteguia, Appl. Catal. B Environ. 48 (2004) 167–174.
[15] C. Bruno, P.M. Walsh, D.A. Santavicca, N. Sinha, Y. Yaw, F.V. Bracco, Combust. Sci. Technol. 31 (1983) 43–74.

[16] S. Karagiannidis, J. Mantzaras, G. Jackson, K. Boulouchos, *Proc. Combust. Inst.* 31 (2007) 3309–3317.

[17] M. Reinke, J. Mantzaras, R. Bombach, S. Schenker, A. Inauen, *Combust. Flame* 141 (2005) 448–468.

[18] M. Reinke, J. Mantzaras, R. Schaeren, R. Bombach, A. Inauen, S. Schenker, *Combust. Flame* 136 (2004) 217–240.

[19] M. Reinke, J. Mantzaras, R. Schaeren, R. Bombach, A. Inauen, S. Schenker, *Proc. Combust. Inst.* 30 (2005) 2519–2527.

[20] C. Appel, J. Mantzaras, R. Schaeren, et al., *Combust. Flame* 128 (2002) 340–368.

[21] Z. Qin, V.V. Lissianski, H. Yang, W.C. Gardiner, S.G. Davis, H. Wang, *Proc. Combust. Inst.* 28 (2000) 1663–1669.

[22] M.E. Coltrin, R.J. Kee, F.M. Rupley, *Surface Chemkin: A Fortran Package for Analyzing Heterogeneous Chemical Kinetics at the Solid Surface–Gas Phase Interface*, Report No. SAND90-8003C, Sandia National Laboratories, 1996.

[23] R.J. Kee, F.M. Rupley, J.A. Miller, *Chemkin II: A Fortran Chemical Kinetics Package for the Analysis of Gas-Phase Chemical Kinetics*, Report No. SAND89-8009B, Sandia National Laboratories, 1996.

[24] R.J. Kee, G. Dixon-Lewis, J. Warnatz, M.E. Coltrin, J.A. Miller, *A Fortran Computer Code Package for the Evaluation of Gas-Phase Multicomponent Transport Properties*, Report No. SAND86-8246, Sandia National Laboratories, 1996.

[25] C. Appel, J. Mantzaras, R. Schaeren, R. Bombach, A. Inauen, *Combust. Flame* 140 (2005) 70–92.

[26] M. Reinke, J. Mantzaras, R. Schaeren, R. Bombach, W. Kreutner, A. Inauen, *Proc. Combust. Inst.* 29 (2002) 1021–1029.

[27] M. Reinke, Mantzaras, R. Bombach, S. Schenker, N. Tylli, K. Boulouchos, *Combust. Sci. Technol.* 179 (2007) 553–600.

[28] P.A. Bui, D.G. Vlachos, P.R. Westmoreland, *Proc. Combust. Inst.* 26 (1996) 1763–1770.

[29] G. Jomaas, X.L. Zheng, D.L. Zhu, C.K. Law, *Proc. Combust. Inst.* 30 (2005) 193–200.